Journal of Pharmaceutical and Medical Research
Print ISSN: 2663-1954
Online ISSN: 2663-1962
DOI: https://doi.org/10.61784/jpmr3105

HOT-AIR DRYING OF MEDICINAL MATERIALS BASED ON COUPLED HEAT-MOISTURE AND MOVING-BOUNDARY MODELS

YinLei Dong
School of Science, Yanshan University, Qinhuangdao 066000, Hebei, China.

Abstract: Hot-air drying of cylindrical medicinal materials couples heat conduction, moisture diffusion, and shrinkage, so a fixed-geometry model may misestimate drying completion. This study develops a radial heat-moisture model that progresses from constant properties to temperature- and moisture-dependent properties and an arbitrary Lagrangian-Eulerian (ALE) moving boundary. A vertex-centred finite-volume scheme, Rannacher-started Crank-Nicolson integration, Picard iteration, and diffusion-potential interface fluxes are used; ambient temperature is fitted with a Weibull function, and grid and balance checks assess numerical consistency. In the constant-property baseline at 1,800 s, center and surface temperatures are 33.5753 and 36.7856 °C, with moisture contents of 2.5500 and 1.5102 kg/kg. At 3 h, the variable-property model predicts 49.8495 and 49.9664 °C and moisture contents of 1.7662 and 1.0081 kg/kg. The maximum-moisture endpoint is 57.4730 h for fixed radius and 51.0852 h with shrinkage as radius falls from 2.0 to 1.2 cm. Temperature-fit RMSE is 0.1447 °C (R^2 = 0.999197). The results indicate that moving geometry changes predicted process duration; internal moisture and radius measurements are needed to validate the estimates beyond the tested assumptions.
Keywords: Hot-air drying; Medicinal materials; Heat-moisture coupling; Finite volume method; Weibull temperature model; Moving boundary

1 INTRODUCTION

Drying is a typical post-harvest operation for medicinal materials; otherwise, they may be damp and not suitable for storage or use. Hot-air drying is chosen due to the relatively simple equipment and operating control, but the process time and quality are affected by coupled heat transfer and water migration in the material. A cylindrical medicinal material with a wet core and an exposed surface will form radial gradients; the surface responds first to the air boundary, and the centre may still be above the target moisture level. Water loss will cause the material to contract and alter both the diffusion path length and the configuration of the heat and mass transfer problem.

Recent studies have investigated hot-air drying equipment for Fritillaria ussuriensis and medicinal Neem leaves [1-2], as well as solar-assisted drying of Giloy [3]. Numerical and process-simulation studies have addressed hot-air drying of shiitake mushrooms [4], ALE-based shrinkage during convective drying of banana slices [5], hybrid ultrasound-convective drying [6], and mint drying [7]. ALE modeling has also been applied to potato dehydration [8]. Recently, some research on the drying kinetics and bioactive compound retention of medicinal plants has been published [9], along with a two-dimensional numerical study of coupled heat and moisture transfer [10]. Collectively, these studies motivate models that can address internal gradients, material-property variation and geometric change.

This paper studies the hot-air drying of a cylindrical medicinal material that is originally 25 cm long and has a radius of 2.0 cm at 28 °C and a dry-basis moisture content of 2.55 kg/kg. It asks how radial temperature and moisture change under constant and state-dependent properties, how long it takes for the material to reach a full-field moisture threshold of 0.15 kg/kg, and how shrinkage affects that endpoint. The focus is not an average-moisture estimate; instead, the maximum internal moisture is tracked so that the last-wetting region is included in the completion criterion.

Radial Heat and Moisture Conservation Equations are used to build this study. A fixed-radius constant-property model provides the early-stage baseline; a variable-property model then couples local temperature and moisture with density, heat capacity, conductivity and diffusivity. For long-term drying, the ambient-temperature boundary is fitted by a Weibull-type function. An ALE coordinate maps the shrinking radius to a fixed computational interval, and a conservative finite-volume scheme includes diffusion and mesh-motion fluxes. Rannacher startup, Crank-Nicolson time stepping and Picard iteration are applied, and grid refinement and reported balance checks are used to assess numerical behaviour.

A fixed-radius and moving-boundary simulation are used to quantify the effect of size reduction on predicted drying time. Based on the above analysis, a process model is established to select a suitable drying time and identify any assumptions or extrapolation limits for future experiments. The interpretation is subject to parameterisation and geometry; experiments to measure changes in radius and spatial moisture should be conducted to validate the predicted schedule before applying this method to other materials or dryers.

2 RELATED STUDIES AND SCOPE

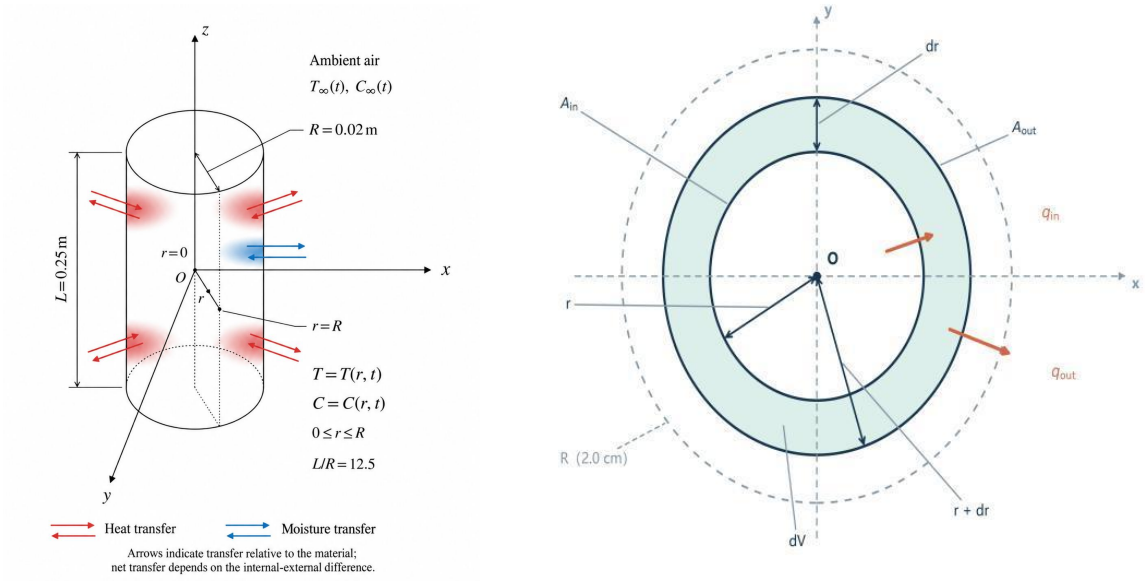
© By the Author(s) 2026, under the CC BY-NC-ND license (http://creativecommons.org/licenses/by-nc-nd/4.0).

Recent studies on the drying of medicinal plants have proposed special equipment and drying methods for herbs [1-3, 9]; numerical simulations have modelled hot-air process simulation [4], ALE-based shrinkage [5], hybrid convective drying [6], mint drying [7], and coupled heat-moisture transfer or geometric change [8, 10]. The present analysis combines the above lines of inquiry with explicit radial heat-moisture coupling and an empirical moving radius, and then compares endpoint predictions under fixed and shrinking geometries.

3 MODEL FORMULATION AND NUMERICAL METHOD

3.1 Geometry and Assumptions

The material is a long cylinder with an initial length of 0.25 m and a radius of 0.020 m. As the length is 12.5 times that of the radius, and the desired outputs are radial, end effects are ignored; therefore, temperature and dry-basis moisture are considered axisymmetric. The porous material is treated as homogeneous, continuous, isotropic and in local thermal equilibrium. Dryer air is uniform around the material. Latent heat of evaporation, adsorption/desorption heat, radiation, internal pressure-driven flow and reaction heat are not considered. The initial temperature is 28°C (301.15 K), and the initial dry-basis moisture content is 2.55 kg/kg. The centreline is a zero-flux symmetry boundary; convective heat and mass transfer occur at the outer surface. The geometry of the cylinder and annular control volume are shown in Figure 1, and the basic dimensions and properties are listed in Table 1.



(a) (b)

Figure 1 (a) Cylindrical Material and Radial Heat-Moisture Transfer; (b) Annular Control-Volume Geometry Used in the Radial Model

Table 1 Geometry and Constant-Property Baseline Parameters

Parameter	Value	Unit or meaning
Initial length; radius	0.25; 0.020	m
Initial temperature; dry-basis moisture	28; 2.55	°C; kg/kg
Density; specific heat	820; 2,600	kg/m³; J/(kg·K)
Thermal conductivity	0.36	W/(m·K)
Surface heat-transfer coefficient	25	W/(m²·K)
Surface mass-transfer coefficient	8×10^{-7}	m/s

3.2 Coupled Radial Conservation Equations

The Temperature Field satisfies energy conservation in cylindrical coordinates, and the dry-basis moisture field is governed by an effective Fickian diffusion law. The local density, heat capacity, conductivity and diffusivity may be constant in the baseline model or state-dependent in the coupled formulation.

$$\rho(C)\, c_p(C)\, \frac{\partial T}{\partial t} = \frac{1}{r}\frac{\partial}{\partial r}\left[r\, k(C)\, \frac{\partial T}{\partial r}\right] \quad (1)$$

$$\frac{\partial C}{\partial t} = \frac{1}{r}\frac{\partial}{\partial r}\left[r\, D(C,T)\, \frac{\partial C}{\partial r}\right] \quad (2)$$

For the constant-property stage, the effective moisture diffusivity depends on the moisture content. The extended model updates material properties according to the local temperature and moisture; the temperature in the diffusivity relation is in kelvins.

$$D(C) = 7 \times 10^{-9} \exp\left(-0.89\frac{1}{C}\right)\ m2^{/s} \quad (3a)$$

$$\rho(C) = 650 + 128\,C \tag{3b}$$
$$c_p(C) = 1450 + 2736\,\frac{C}{C+1} \tag{3c}$$
$$k(C) = 0.21 + 0.38\,\frac{C}{C+1} \tag{3d}$$
$$D(C,T) = 2.4 \times 10^{-3} \exp\left(\frac{-0.45}{C} - \frac{3850}{T}\right) \tag{3e}$$

3.3 Ambient Temperature and Drying Criterion

The measured ambient temperature and equivalent air-moisture series are linearly interpolated between observations for early-stage calculations. A Weibull-type function is used to fit the 241 temperature observations of long-duration drying, starting at 28°C and asymptotically approaching 50°C. As the governing equations use kelvins, the fitted Celsius curve needs to be converted before use; thus, the boundary is approximately 323.15 K.

$$T_\infty(t) = 323.15 - 22 \exp\left[-\left(\frac{t}{1881.244}\right)^{1.152732}\right] \tag{4}$$

The fitted characteristic time is 1,881.244 s and the shape parameter is 1.152732. Drying is deemed to be finished only when the maximum internal moisture in all parts of the material has reached a certain limit; therefore, the centre usually dries last.

$$C_{max}(t) = \max_{0 \le r \le R_t}\big(C(r,t)\big) \tag{5a}$$
$$t_{end} = \inf\{t : C_{max}(t) \le 0.15\ kg/kg\} \tag{5b}$$

3.4 Spatial Discretization and Time Integration

A vertex-centred finite-volume method is used for the radial control volumes. A complete control volume with zero central flux is employed to represent the center and thus avoid direct evaluation at the cylindrical-coordinate singularity. Rannacher startup takes two backward-Euler half-steps first, then a Crank-Nicolson advance. Picard iteration updates the nonlinear term, and then a Thomas algorithm solves the resulting tridiagonal system. For long-horizon fixed-radius drying, adaptive implicit Crank-Nicolson stepping and diffusion-potential interface fluxes are used; an eight-point Gauss-Legendre rule evaluates the diffusion-potential integral.

3.5 Moving-Boundary ALE Formulation

A Piecewise-linear interpolation is used to represent the measured radius history. The ALE coordinate maps the shrinking physical interval to a fixed computational interval, and thus the conservation law can consider both material diffusion and mesh motion.

$$\xi = \frac{r}{R(t)},\ r = R(t)\,\xi,\ 0 \le \xi \le 1 \tag{6}$$
$$\frac{d}{dt}\left[R^2 V_i^{\xi} C_i\right] + \Phi_{i+1/2} - \Phi_{i-1/2} = 0 \tag{7}$$

Sum the discrete moisture balance for all control volumes and cancel the internal interface fluxes. As the centre flux is zero, only surface transfer affects the total moisture; thus, mesh motion does not generate or eliminate water numerically. If the radius change is set to zero, then the ALE form becomes a fixed-radius model.

4 RESULTS

4.1 Early-Stage Profiles

After 1,800 s in the constant-property baseline, the center and surface temperatures are 33.5753 °C and 36.7856 °C, and the moisture contents are 2.5500 and 1.5102 kg/kg. After 3 h of the variable-property coupled model, the centre and surface temperatures were 49.8495°C and 49.9664°C, respectively, and the corresponding moisture contents were 1.7662 kg/kg and 1.0081 kg/kg. Therefore, the reduction in surface moisture occurs earlier than that of the core, and then the temperature field gradually tends to be uniform with the ambient temperature. The representative centre and surface results are listed in Table 2 below.

Table 2 Center and Surface Results at Representative Early Times

Model stage	Time	Temperature center / surface (°C)	Moisture center / surface (kg/kg)
Constant-property baseline	1,800 s	33.5753 / 36.7856	2.5500 / 1.5102
Variable-property coupled model	3 h	49.8495 / 49.9664	1.7662 / 1.0081

4.2 Fixed-Radius Long-Duration Drying

The Weibull boundary-temperature fit has an RMSE of 0.1447 °C, a MAE of 0.1239 °C, and an R^2 of 0.999197 for the fitted observations. A 3-4 hour hold-out extrapolation has an RMSE of 0.1523°C; first-order inertia and OU state-space alternatives have errors of 0.1542°C and 0.1729°C, respectively. Table 3 shows the fitting and short-horizon forecast errors of the reported models.

Table 3 Ambient-Temperature Model Fit and Short-Horizon Extrapolation

Model	Fit RMSE (°C)	MAE (°C)	R^2	3-4 h forecast RMSE (°C)
Weibull	0.1447	0.1239	0.999197	0.1523
First-order inertia	0.3699	0.2914	0.994748	0.1542
OU state-space	0.4178	0.3359	0.993300	0.1729

At a constant radius, moisture first decreases near the surface and then moves inward. The volume-average moisture is less than 0.15 kg/kg before the maximum moisture; thus, using an average as the endpoint criterion may end drying when the center has not yet reached the target. The fixed-radius drying time based on the maximum-moisture criterion is 57.4730 h. Figure 2 shows the distribution of moisture and the separation between full-field and volume-average endpoint detection.

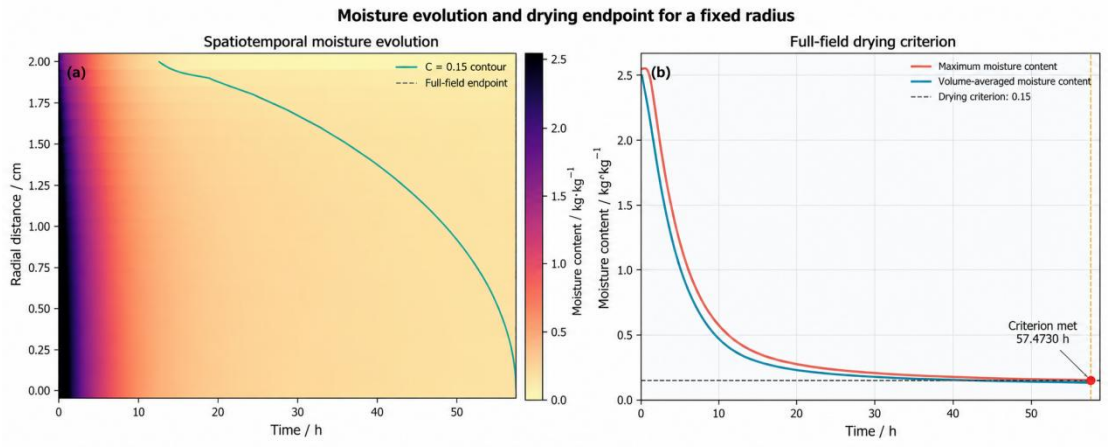


Figure 2 Fixed-Radius Moisture Evolution and Full-Field Endpoint Criterion

4.3 Shrinking-Radius Drying

The ALE simulation is in line with the measured radius history. The radius is approximately 1.3 cm at 6 h and 1.2 cm from 12 h onwards. At the reported endpoint, the centre moisture is 0.1500 kg/kg and the surface moisture is 0.0526 kg/kg; other reported radial positions are below the threshold. The drying time for a shrinking-radius model is 51.0852 h, compared with 57.4730 h for a fixed-radius model; that is to say, it has decreased by about 11.11%. Figure 3 shows the moving moisture field and the endpoint-time comparison. Table 4 compares the endpoint predictions for fixed and shrinking geometries.

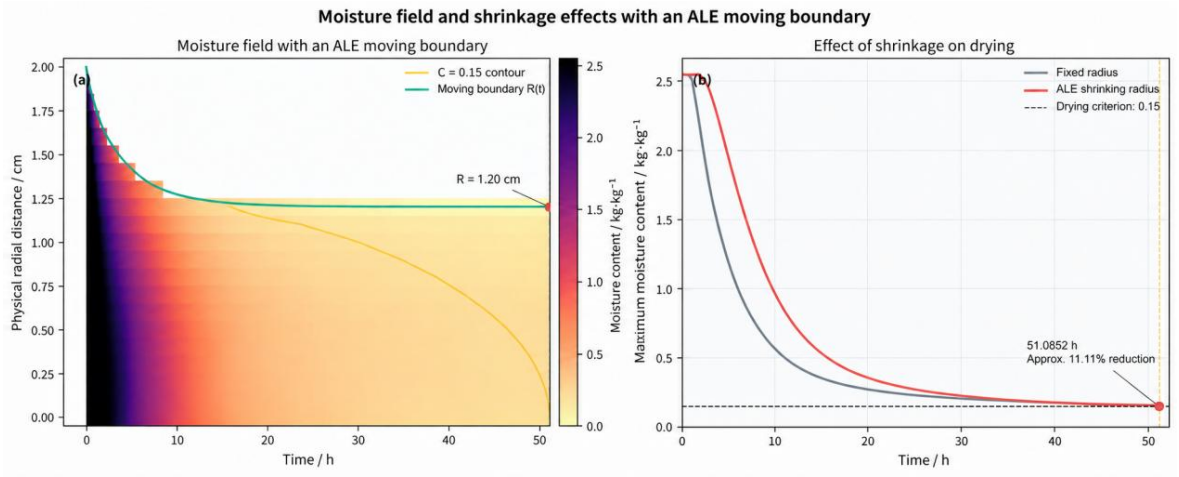


Figure 3 ALE Moisture Field and Drying-Time Comparison Under Radius Shrinkage

Table 4 Fixed-Radius and Moving-Boundary Endpoint Predictions

Model	Completion time (h)	Final radius (cm)	Center moisture at threshold (kg/kg)	Time change
Fixed radius	57.4730	2.0	0.1500	Reference
ALE shrinking radius	51.0852	1.2	0.1500	-11.11%

4.4 Numerical Convergence

At a 2 s time step, the ALE endpoint estimates for 160, 320 and 640 radial control volumes are 51.0634 h, 51.0806 h and 51.0852 h. Successive differences decrease from 0.0172 h to 0.0046 h, and the reported observed mesh order is approximately 1.91. The report warns that the upwind mesh-motion flux cannot be considered strictly second-order, but the 640-cell result shows good grid independence. Figure 4 and Table 5 show the results of this convergence check.

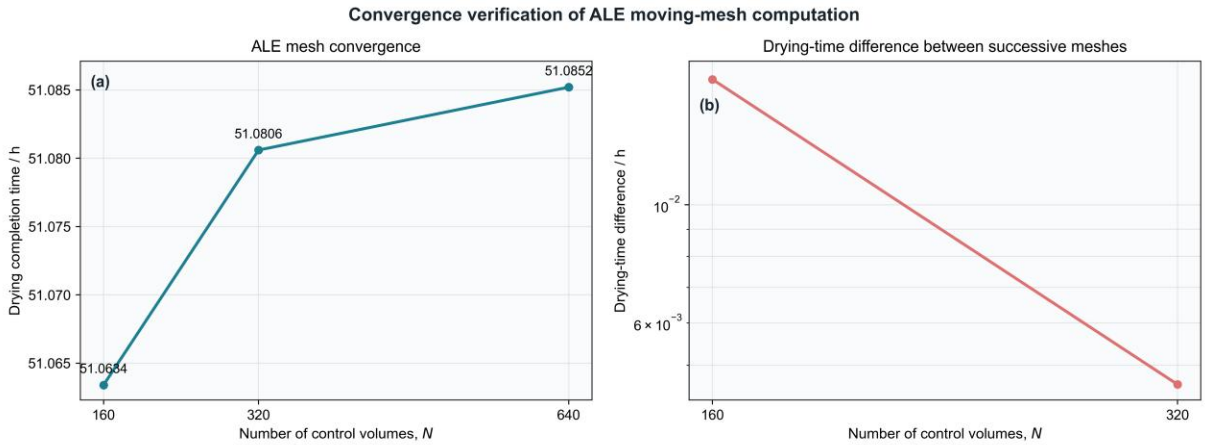


Figure 4 ALE Endpoint Convergence with Increasing Radial Control Volumes

Table 5 ALE Grid-Convergence Results

Radial control volumes	Endpoint time (h)	Change from preceding grid (h)
160	51.0634	-
320	51.0806	0.0172
640	51.0852	0.0046

For the variable-property coupled stage, the reported Picard iteration averaged 2.0715 and had a maximum of three. The cumulative equivalent-moisture and heat-balance relative errors were 2.1609 × 10^-13 and 9.1153 × 10^-12, respectively. Spatial and temporal convergence orders near two for temperature and moisture fields were obtained in the early mesh tests.

5 CONCLUSION

The results show that the model can track radial heat and moisture fields while accounting for material-property changes and measured shrinkage. Under the reported assumptions, the full-field endpoint decreases from 57.4730 h for the fixed-radius case to 51.0852 h for the ALE case as radius contracts from 2.00 to 1.20 cm; grid refinement and balance checks support numerical consistency. This establishes the feasibility of using a moving-boundary finite-volume model to assess drying completion in cylindrical materials. The comparison is model-based and does not establish a production-time saving. Its current scope is limited to one-dimensional axisymmetric transport, uniform air conditions, and empirical boundary and shrinkage histories; internal moisture predictions have not been validated by direct measurement. Future experiments should measure radial moisture and temperature profiles, radius evolution, and dryer-air conditions throughout drying. Those data can test the endpoint criterion and refine surface-transfer coefficients and shrinkage relations. Further tests should examine other medicinal materials, cylinder sizes, dryer conditions, and nonuniform deformation. This validation will show when the model can provide reliable process-time estimates and whether axial or stress-coupled models are needed.

COMPETING INTERESTS

The authors have no relevant financial or non-financial interests to disclose.

REFERENCES

[1] Wu L, Qi J, Sun L, et al. Design of and experimental study on drying equipment for Fritillaria ussuriensis. Applied Sciences, 2025, 15(15): 8427.

[2] Sinha R, Thakur A D, Raj R. Investigating drying behavior and quality of Neem leaves using a novel biomass gasification-powered climate control unit with built-in humidity control. International Communications in Heat and Mass Transfer, 2024, 158: 107888.

[3] Yadav D K, Arora V K, Gupta A. Experimental investigation on the thermal appraisal and sustainability indicator of heat pipe-based indirect solar dryer during Giloy (Tinospora cardifolia) drying. Thermal Science and Engineering Progress, 2024, 47: 102335.

[4] Sun D, Hu R, Wang P, et al. Integrated simulation method construction and process optimization for hot air drying of shiitake mushrooms. LWT, 2024, 206: 116577.

[5] Das R, Islam M, Saini P, et al. Finite element modeling of banana slices in convective drying, studies on isotropic shrinkage kinetics using Arbitrary Lagrangian-Eulerian (ALE) approach. Thermochimica Acta, 2025, 749: 180024.
[6] Chen K K, Torki M, Ghanbarian D, et al. Numerical simulation and study on heat and mass transfer in a hybrid ultrasound/convective dryer. Journal of Food Science and Technology, 2024, 61(6): 1094-1104.
[7] Kaveh M, Zomorodi S, Szymanek M, et al. Determination of drying characteristics and physicochemical properties of mint (Mentha spicata L.) leaves dried in refractance window. Foods, 2024, 13(18): 2867.
[8] Das R, Prasad K. Finite element modeling in heat and mass transfer of potato slice dehydration, nonisotropic shrinkage kinetics using arbitrary Lagrangian-Eulerian algorithm and artificial neural network. Journal of Food Process Engineering, 2024, 47(2): e14545.
[9] Suresh K, Kumaraswamy M, Sundaravadanam H, et al. Engineering perspectives on drying technologies of medicinal plants: A review on kinetic modelling and bioactive compounds retention. Applied Science and Engineering Progress, 2026, 19(1): 7900.
[10] Ali I. Two-dimensional numerical modeling and simulation of heat and moisture transfer during drying. AIMS Mathematics, 2026, 11(3): 8762-8791.